Journal of Power Sources 200 (2012) 53–58

Contents lists available at SciVerse ScienceDirect

Journal of Power Sources

journal homepage: www.elsevier.com/locate/jpowsour

Composite lithium battery anodes based on carbon@Co_3O_4 nanostructures: Synthesis and characterization

Navaneedhakrishnan Jayaprakash, Wanda D. Jones, Surya S. Moganty, Lynden A. Archer*

School of Chemical and Biomolecular Engineering, Cornell University, Ithaca, NY 14853-5201, USA

ARTICLE INFO

Article history:
Received 19 August 2011
Received in revised form 4 October 2011
Accepted 6 October 2011
Available online 13 October 2011

Keywords:
C@Co_3O_4 anode
Composite
LIB application
Hydrothermal
High rate discharge

ABSTRACT

We report on the formation of carbon/Co_3O_4 (C@Co_3O_4) composite nanospheres using a hydrothermal approach, followed by application of a thin coating of monosaccharide-derived carbon veneered on the surface of Co_3O_4 by high temperature calcination. When evaluated as the negative electrode for Li-ion batteries (LIBs), the C@Co_3O_4 structures exhibit attractive energy storage capacity and improved cycle life, over more than 100 repeated discharge/charge cycles. We hypothesize that the improved electrochemical performance of the composite electrodes originates from the enhanced structural stability of the active Co_3O_4 particles, imparted by the carbon coating. Consistent with this hypothesis, post mortem analysis performed on pristine Co_3O_4 and composite C@Co_3O_4 anodes subjected to prolonged cycling indicate that surface cracking, particle breakage, and primary particle fusion evident in the pristine Co_3O_4 material are substantially reduced in anodes comprised of C@Co_3O_4.

© 2011 Elsevier B.V. All rights reserved.

1. Introduction

Growing demand for lightweight, reliable secondary batteries that exceed performance of current energy storage technologies for electronics, communication, and aerospace applications [1] have led to significant research and development efforts world-wide. Secondary lithium ion batteries (LIBs) are broadly understood to be the technology platform of choice to meet these needs and are also on the verge of becoming the preferred power source for hybrid electric vehicles (HEVs) and plug-in hybrid vehicles (PHEV). Compared with nickel-metal hydride batteries (now used for many commercial HEVs), LIBs offer superior specific energy and power, which make them attractive for EV applications. To this end, LIBs that employ metal oxides in place of the currently used LiC_6 anodes are receiving intense attention because they potentially offer higher energy and power densities, in many cases at comparable overall cell potentials [2–6].

To obtain a LIB with long cycle life, the anode material should endure repeated lithium insertion and extraction without significant structural damage. Many transition metal oxide anodes undergo significant volume change upon lithium intercalation and exhibit significant capacity fading upon extended cycling [2–6], which has reduced enthusiasm for the materials in commercial LIB systems. Some studies have considered doping or surface modification of metal oxides to circumvent structural deterioration and aggregation of the active particles that occurs over many charge discharge cycles [2,3,7]. Construction of size reduced particles, as well as particles of reduced dimensionalities, have also been studied and found effective in enhancing the electrode performance of some metal oxides [8]. Among the transition metal oxides, Co_3O_4 is an important anti-ferromagnetic intrinsic p-type semiconductor [7,9–17], used as the anode in LIBs [18–24] it has the ability to accommodate up to 8 Li^+ ions per formula unit according to the displacive redox reaction $Co_3O_4 + 8Li \leftrightarrow 4Li_2O + 3Co^0$. The theoretical capacity of Co_3O_4 as per the proposed reaction can be calculated to be 890 mAh g^{-1}, which represents a nearly 150% increase over that delivered by conventional carbonaceous anodes [7,11,23,24]. Since the reaction of Co_3O_4 with Li involves formation and decomposition of Li_2O associated with the reduction and oxidation of the metal oxide/metal particles, nano sized materials are generally considered preferred because they potentially facilitate the decomposition of Li_2O [11].

Herein, we report a facile hydrothermal strategy for synthesizing narrow-size-distribution Co_3O_4 nanoparticles and a solution phase process, followed by high-temperature calcination, for applying a coating of carbon onto the materials. Hydrothermal synthesis of Co_3O_4 has several advantages compared to most conventional techniques, such as simplicity, low processing temperatures, low cost, high product purity, and the ability to control the particle size and morphology. As discussed in our previous works [25], the carbon coating is thought to enhance the structural stability and potentially improve electron transport to the material. When used as the anode in rechargeable Li-ion batteries, the as prepared C@Co_3O_4 composites exhibit a lithium deinsertion

* Corresponding author. Tel.: +1 607 254 8825; fax: +1 607 255 9166.
E-mail address: laa25@cornell.edu (L.A. Archer).

0378-7753/$ – see front matter © 2011 Elsevier B.V. All rights reserved.
doi:10.1016/j.jpowsour.2011.10.018

capacity of 567 mAh g^{-1} at the end of 107 cycles of discharge and charge at a current rate of 445 mA g^{-1} (0.5 C). The material also displays attractive charge rate capabilities. Postmortem and control studies indicate that the improved LIB performance of C@Co_3O_4 composites strongly relies on the presence of the carbon coating.

2. Experimental methods

All chemicals or materials were used directly without any further purification prior to use. Cobalt nitrate hexahydrate ($Co(NO_3)_2{\cdot}6H_2O$; Aldrich, 99.99%), ammonium hydroxide ($NH_3{\cdot}H_2O$, 28–30 wt %, J.T. Baker), polyvinylpyrrolidone (PVP-K30, M_w – 40,000, Aldrich), polyvinylidene fluoride (PVDF, Aldrich), super-p lithium conducting carbon (Timcal), copper foil (9 μm thickness, MTI Corporation, USA) and metallic Li foil (0.75 mm thickness, 99.9%, Aldrich) were used.

2.1. Synthesis of monodispersed pristine and C@Co_3O_4

In a typical synthesis, 37.5 mL of ammonium hydroxide 12.5 mL milli-Q water and 25 mM $Co(NO_3)_2$ were mixed step-by-step under vigorous stirring in a reagent bottle. To the homogenous solution obtained, 1 g PVP-K30 was added and allowed to stir for another 20 min. The resultant dark transparent solution was then transferred to a 50 mL glass lined autoclave (Parr Inc.), tightly sealed and heated at a temperature of 180 °C in a preheated electric oven for 8 h. After the reaction is complete, the autoclave was allowed to cool to room temperature and the resultant precipitate was centrifuged and washed completely with water and ethanol. The powder sample obtained was vacuum-dried at 100 °C. The C@Co_3O_4 nanoparticles were prepared by the method already reported by our group [25]. In a typical carbon coating process, 200 mg of the synthesized Co_3O_4 particles was suspended in 20 mL of 0.15 M glucose (Sigma–Aldrich, 99.99%) solution under ultrasonication for 30 min. Glucose is selected as the carbon precursor since it prevents the chaotic coalescence or aggregation of C@Co_3O_4 nano spheres by favoring particle separation. The resulting suspension was transferred to a 50 mL glass lined autoclave and then heated at 180 °C in a preheated electric oven for 4 h. The partially denatured glucose coated Co_3O_4 was collected via centrifugation and dried at 100 °C and then sintered at 500 °C for 3 h under Ar flow.

2.2. Characterization of the samples

Transmission electron microscopy (TEM, Tecnai, T12, 120 kV), scanning electron microscopy (LEO 1550-FESEM) powder X-ray diffraction (Scintage X-ray diffractometer with Cu Kα radiation), thermogravimetric analysis (under air, Thermo Scientific TA Instrument (Nicolet iS10) operated at a heating rate of 20 °C min^{-1}), cyclic voltammetry (Solartron's Cell Test model potentiostat, potential

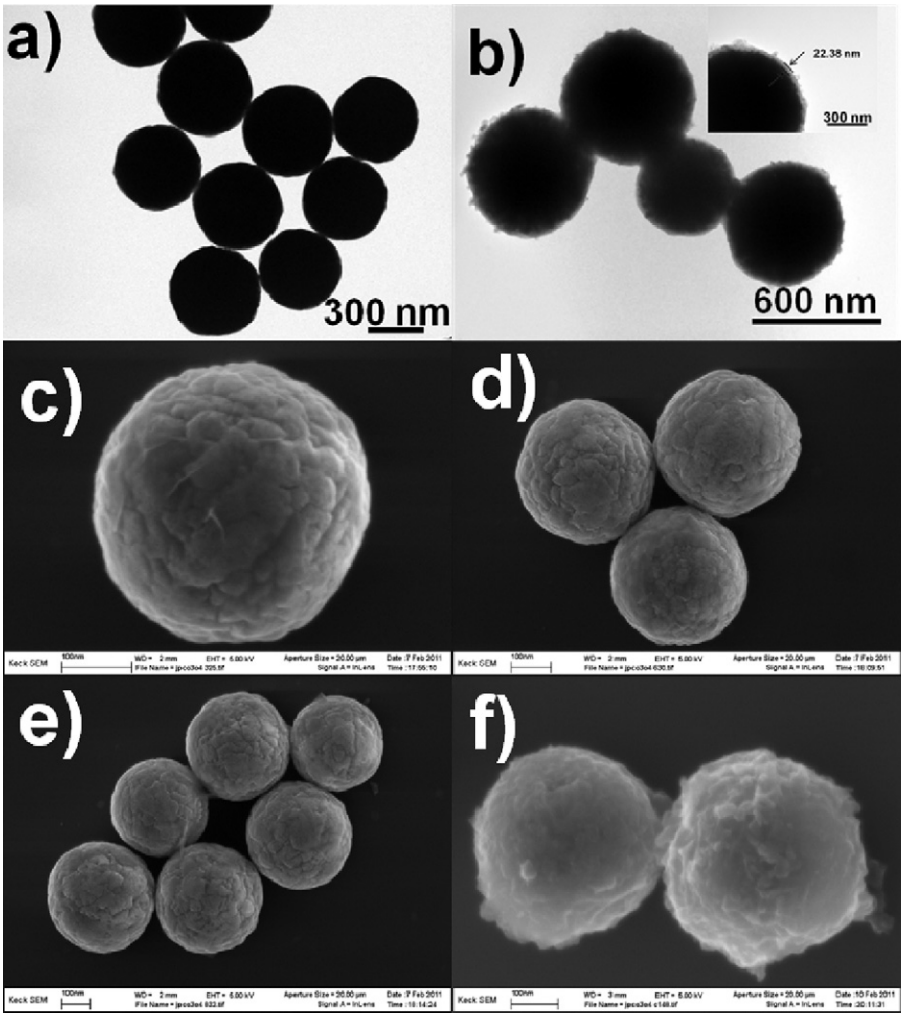

Fig. 1. TEM and SEM images of pristine Co_3O_4 (a, c, d and e) and C@Co_3O_4 (b and f) nano spheres. Inset to (b) shows an ~22 nm thickness of carbon coating upon Co_3O_4 nanospheres.

window 3.0 – 0.5 V/0.2 mV s^{-1}), electrochemical charge discharge analysis (Maccor cycle life tester, under the potential window 3.0–0.5 V).

2.3. Electrode preparation

The pristine and C@Co_3O_4 anode slurry was made by mixing 87.5% of the synthesized C@Co_3O_4 (85% of pristine), 5% super-p lithium conducting carbon (Timcal, 7.5% for pristine) and 7.5% of PVDF (Sigma–Aldrich) binder in NMP (Sigma–Aldrich) dispersant. Negative electrodes were produced by coating the slurry on copper foil and dried at 120 °C for 1 h initially and at 100 °C for 4 h in vacuum oven. The resulting slurry-coated copper foil was roll-pressed and the electrode was reduced to the required dimensions with a punching machine. Preliminary cell tests were conducted on 2032 coin-type cells, which were fabricated in an argon-filled glove box using lithium metal as the counter electrode and a micro porous polyethylene separator. The electrolyte solution was 1 M $LiPF_6$ in 1:1 EC:DEC.

3. Results and discussion

Fig. 1a shows the transmission electron microscopy (TEM) image of the as synthesized Co_3O_4 nano spheres. It is evident from the figure that the synthesis procedure yields uniform, nearly monodisperse, and spherical Co_3O_4 particles with an average diameter of ca. 400–500 nm. A coating of carbon was applied to the surface of the Co_3O_4 particles by solution phase deposition of glucose, followed by high-temperature carbonization. Fig. 1b is a representative TEM image of the C@Co_3O_4 particles, which shows that the coating procedure produces no noticeable change on the particle morphology. A thin, uniform carbon layer of 22 nm in thickness (inset to Fig. 1b) is observed on the surface of the Co_3O_4 particles. To further characterize the surface morphology and size distribution of the pristine and C@Co_3O_4 nanospheres, the samples were evaluated by scanning electron microscopy analysis. Fig. 1c–f represents the SEM images of the pristine and C@Co_3O_4 particles. It is clear from the figure that the particles retain their uniformity and narrow size distribution, which is expected to increase the inter-particular contact area between particles thus reducing the overall internal resistance. The spongy surface shown in Fig. 1f is consistent with uniform carbon coating of the Co_3O_4 nanospheres, in agreement with the result obtained from TEM analysis.

The phase purity and degree of structural order of the pristine Co_3O_4 and C@Co_3O_4 materials were studied using powder X-ray diffraction (XRD) spectrum (Fig. 2a). The XRD spectrums obtained are consistent with existence of phase pure Co_3O_4 cubic spinel structure with *Fd*3*m* space group (JCPDS File No. 781969). The XRD spectrum for the C@Co_3O_4 is noticeably silent for 2θ values close to 26°, an indication that the coating is comprised of disordered carbon. The diffraction peak intensities for the C@Co_3O_4 particles are also lower that for the pristine Co_3O_4, which is consistent with expectations for the presence of amorphous carbon coating on the surface of the particles. Thermogravimetric analysis (Fig. 2b) of the as prepared C@Co_3O_4 particles indicates that approximately 12 wt% of the material is carbon.

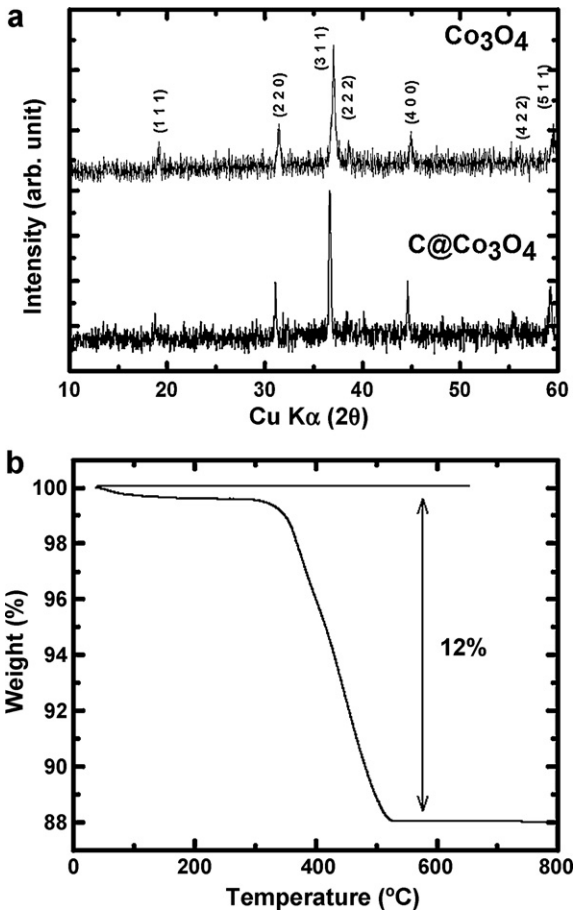

Fig. 2. (a) XRD patterns of Co_3O_4 and C@Co_3O_4 nano spheres, (b) thermo gravimetric analysis plot of C@Co_3O_4 displaying the presence of 12% carbon.

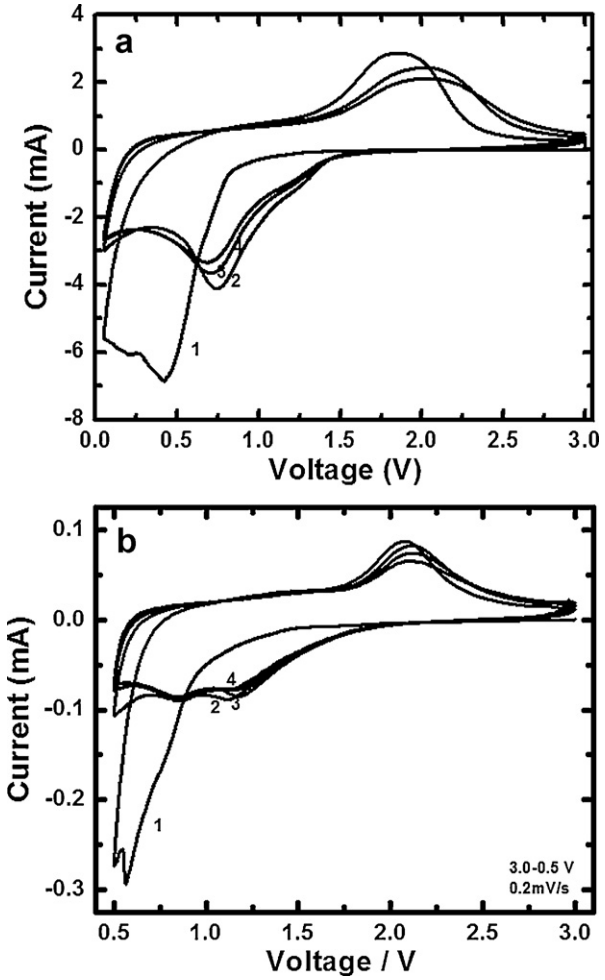

Fig. 3. Typical cyclic voltammograms of (a) Co_3O_4 and (b) C@Co_3O_4 at a sweep rate of 0.2 mV s^{-1}.

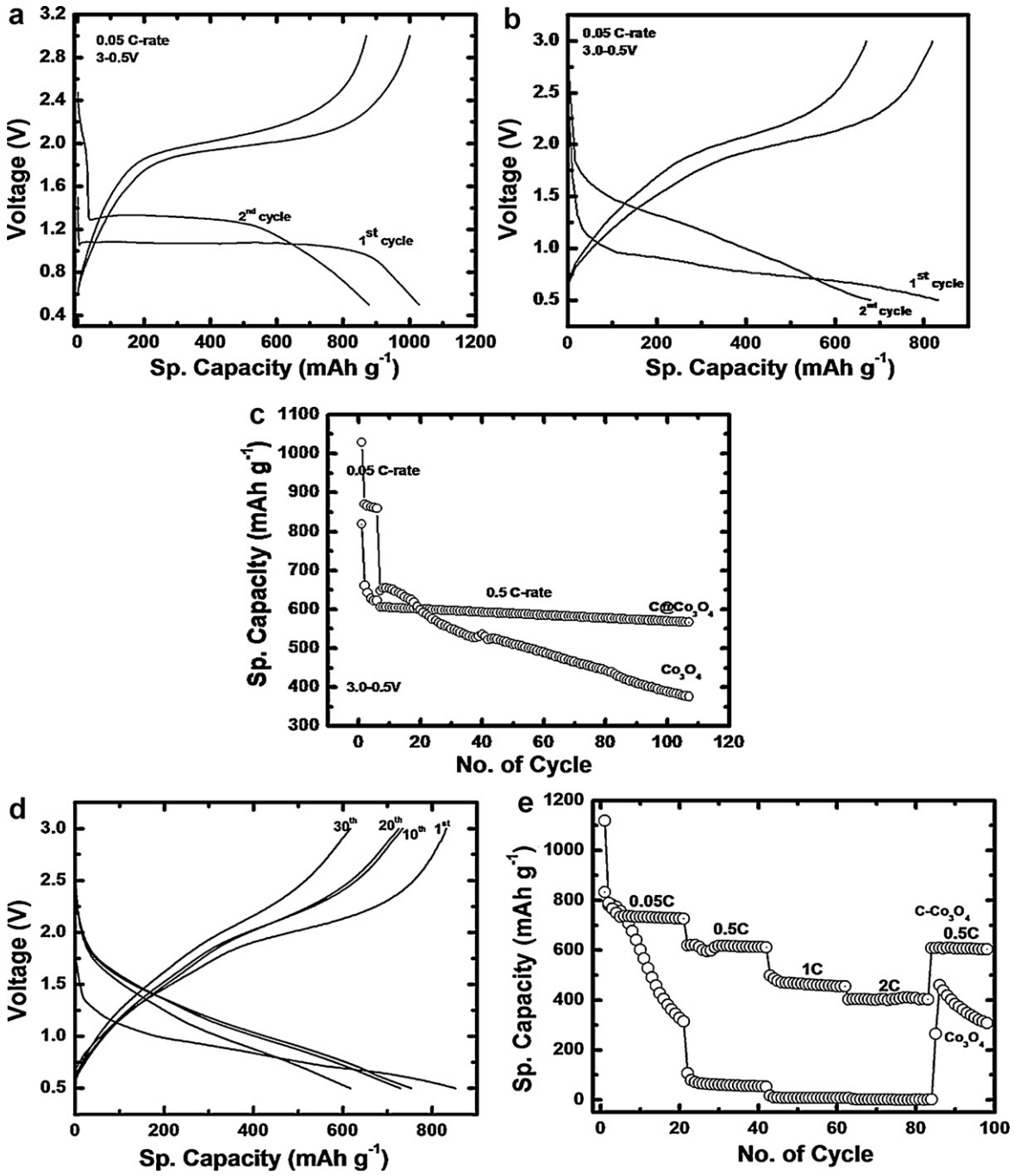

Fig. 4. Voltage *vs.* capacity profiles of (a) Co_3O_4 and (b) C@Co_3O_4 under the potential window 3.0–0.5 V and at 0.05-C rate, (c) capacity *vs.* cycle number plot of pristine and C@Co_3O_4. (d and f) The rate capability study of pristine and C@Co_3O_4 samples. The capacity is reported here in terms of the percentage of the Co_3O_4 active mass.

To evaluate the material as a LIB anode, electrochemical properties were examined by cyclic voltammetry and galvanostatic cycling analysis. Fig. 3a and b shows the cyclic voltammograms of electrodes made from pristine Co_3O_4 and C@Co_3O_4 at room temperature. Both materials were studied in the potential range of 3.0–0.5 *vs.* Li/Li^+ at a scan rate of 0.2 mV s^{-1}. The first cathodic scan of both the pristine Co_3O_4 and C@Co_3O_4 material (Fig. 3b) exhibits an irreversible reduction peak at ~0.5 V, which is attributed to electrolyte decomposition and formation of SEI layer [26]. After the first scan, the CV patterns of both the pristine and carbon-coated materials shows two cathodic peaks at ~1.12 V and ~0.86 V and a corresponding anodic peak at ~2.1 V. Since Co_3O_4 adopts the normal spinel structure with Co^{2+} ions in tetrahedral interstices and Co^{3+} ions in the octahedral sites of the cubic close packed lattice of oxide anions, the reduction/oxidation reaction of the $Co^{2+/3+}/Co^0$ is a complex multi-step process [27]. The pair of cathodic peaks, though not clearly visible, in the pristine Co_3O_4 is merged in the extended scans. This can be compared with the results for the C@Co_3O_4 composites, which show nicely overlapping redox peaks upon extended scans. This is an indication that the synthesized C@Co_3O_4 anode material exhibits improved electrochemical stability.

To further evaluate the electrochemical properties of the C@Co_3O_4 material galvanostatic discharge/charge reactions were performed in the cell voltage of 3.0–0.5 V at various current densities. For the typical cycle life study, the cells were discharged and

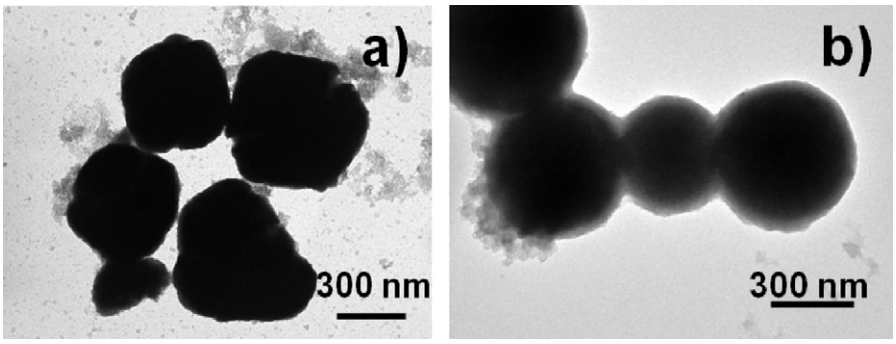

Fig. 5. TEM images of (a) pristine Co_3O_4 and (b) C@Co_3O_4 particles after 107 discharge/charge cycles.

charged initially at a current density of 44 mA g^{-1} (0.05-C rate) for the first five cycles and at 440 mA g^{-1} (0.5-C rate) from 6th to the final cycle. Fig. 4a and b displays the voltage *vs.* capacity plots of the pristine and C@Co_3O_4 materials. It is seen that the lithium insertion/deinsertion plateaus for both materials are similar to previous reports [8,23,24], indicating that they follow a similar redox reaction pathway. It is interesting to note that the Li^+ ion insertion plateau of the C@Co_3O_4 material is not as well defined as for pristine Co_3O_4. This may be attributed to the decrease in crystallinity of the metal oxide upon carbon coating. Initially, the pristine and C@Co_3O_4 material exhibited a Li^+ ion deinsertion capacity of 1029 and 818 mAh g^{-1}, which drastically reduced to 870 and 671 mAh g^{-1} in the second cycle. The first cycle columbic efficiency was calculated to be 97.6% and 98.3%, for the pristine and C@Co_3O_4 materials, respectively. The large difference in the discharge capacity values between the first and second cycle in both the pristine and C@Co_3O_4 may be attributed to the formation of the SEI film and further lithium consumption via interfacial reactions, due to the charge separation at the metal/Li_2O phase boundary [28,29]. Fig. 4c shows the Li^+ ion deinsertion cycling performance of the pristine and C@Co_3O_4 samples. Though the initial capacity of the pristine Co_3O_4 was 1029 mAh g^{-1}, it is seen to fade noticeably to eventually give a capacity of 376 mAh g^{-1} at the end of 107 cycles. In contrast, the C@Co_3O_4 electrode maintains a high degree of reversibility, and its capacity at the end of 107 cycles was found to be 567 mAh g^{-1}. We attribute this observation to the flexible structure provided by carbon coating, which facilitates Li^+ ion insertion/deinsertion while maintaining good ion transport during cycling. Further, the presence of thin layer of amorphous carbon on the surface of Co_3O_4 spheres minimizes the risk of side reactions and restricts the volume expansion of the metal oxide particle thereby preventing the pulverization of the electrode. The carbon layer, which is expected to have good electronic conductivity also act as efficient electrically conductive networks which stabilizes the formed SEI film without decomposition during each discharge and charge process to consume the stored Li capacity [29,30].

Fig. 4d and e illustrates the performance of the pristine and carbon-coated materials in a range of C-rates. It is apparent that the C@Co_3O_4 electrode displays greatly improved rate performance, in particular, when the cell is discharged and charged at 2-C rate, the specific capacity of the electrode based on C@Co_3O_4 manifests a capacity of 423 mAh g^{-1} (Fig. 4e), which is more than 50% of the initial capacity of Co_3O_4. By contrast, the Li^+ ion deinsertion capacity of the pristine Co_3O_4 electrode is observed to drop significantly at high C rates and reaches a value less than 50 mAh g^{-1} at the 2-C current rate. The improved reversibility of the C@Co_3O_4 is also evidenced by the fact that the capacity of 615 mAh g^{-1} at 0.5-C current rate was regained when the rate was lowered to 0.5-C after Li^+ ion deinsertion at 2-C rate of discharge and charge, as shown in Fig. 4e. The stark contrast between the behaviors seen in pristine Co_3O_4 and C@Co_3O_4, in terms of cycle life or rate capability behavior, indicates that the improved electrochemical performance is produced by carbon coating.

To understand the effect of carbon coating in enhancing the electrochemical behavior of Co_3O_4 nanoparticles, the morphology and microstructure variation of both the pristine and C@Co_3O_4 composite particles were examined using TEM after 107 discharge/charge cycles (Fig. 5a and b). As discussed earlier, prior to electrochemical analysis, the surface morphology of the pristine and C@Co_3O_4 materials exhibit good shape and size uniformity. However, it is apparent from the postmortem analysis that the morphology of the pristine Co_3O_4 particles (Fig. 5a), after 107 discharge/charge cycles, undergoes drastic change, both in terms of shape and size; with substantially aggregated and broken particles readily apparent. In contrast, the postmortem analysis of the C@Co_3O_4 (Fig. 5b) materials demonstrate that repeated insertion/deinsertion of Li^+ ions into/from the metal oxide crystal lattice structure has minimal effect on the active particle size or shape. Remarkably, we do not observe a single broken or aggregated C@Co_3O_4 after extended cycling of the material, which underscores the crucial role the carbon coating plays in mechanically stabilizing the material during repeated lithium insertion and deinsertion reactions.

4. Conclusion

In conclusion, we report on the hydrothermal synthesis of nearly monodispersed Co_3O_4 spheres with diameters in the range 400–500 nm. By treating the particles with a polysaccharide solution followed by high-temperature calcination, we further show that a carbon layer of 22 nm in thickness can be coated on the Co_3O_4 particles, to create C@Co_3O_4 hybrid particles with ~12 wt% carbon. By analogy to our previous studies with SnO_2 nanostructures [25], we theorize that the carbon coating should improve the mechanical integrity of the particles and should enhance their structural stability upon the repeated lithium insertion/de-insertion processes that must occur in a lithium ion battery. When evaluated as the anode material for LIB applications, the C@Co_3O_4 composite particles exhibit a Li^+ ion deinsertion capacity of 567 mAh g^{-1} at the end of 107 cycles at 0.5-C rate. Additionally, we find that the as-prepared C@Co_3O_4 composite particles manifest promising rate capability behavior with specific Li^+ ion deinsertion capacities of 738, 615, 444 and 423 mAh g^{-1} at 0.05-, 0.5-, 1- and 2-C rates, respectively. Postmortem analysis of the pristine Co_3O_4 and C@Co_3O_4 composite materials conducted after extended cycling studies for 107 discharge/charge cycles show that while the C@Co_3O_4 retains its morphology, the pristine material does not.

Acknowledgement

This material is based on work supported as part of the Energy Materials Center at Cornell, an Energy Frontier Research Center

funded by the U.S. Department of Energy, Office of Basic Energy Sciences under Award Number DE-SC0001086.

References

[1] J.M. Tarascon, M. Armand, Nature 414 (2001) 359.
[2] W.M. Zhang, X.L. Wu, J.S. Hu, Y.G. Guo, L.J. Wan, Adv. Funct. Mater. 18 (2008) 3941.
[3] Y. Sharma, N. Sharma, G.V. Subba Rao, B.V.R. Chowdari, Adv. Funct. Mater. 17 (2007) 2855.
[4] J.B. Goodenough, Y. Kim, J. Power Sources 196 (2011) 6688.
[5] B. Scrosati, J. Garche, J. Power Sources 195 (2010) 2419.
[6] X.W. Lou, L.A. Archer, Z. Yang, Adv. Mater. 20 (2008) 3987.
[7] Z.S. Wu, W. Ren, L. Wen, L. Gao, J. Zhao, Z. Chen, G. Zhou, F. Li, H.M. Cheng, ACS Nano 4 (2010) 3187.
[8] G. Binotto, D. Larcher, A.S. Prakash, R.H. Urbina, M.S. Hedge, J.M. Tarascon, Chem. Mater. 19 (12) (2007) 3032.
[9] X. Wang, L. Yu, X.L. Wu, F. Yuan, Y.G. Guo, Y. Ma, J. Yao, J. Phys. Chem. 113 (2006) 15553.
[10] S.A. Needham, G.X. Wang, K. Konstantinov, Y. Tournayre, Z. Lao, H.K. Liu, Electrochem. Solid-State Lett. 9 (7) (2006) A315.
[11] B. Guo, C. Li, Z.Y. Yuan, J. Phys. Chem. C 114 (2010) 12805.
[12] M.V. Reddy, Z. Beichen, L.J. Nicholette, Z. Kaimeng, B.V.R. Chowdari, Electrochem. Solid-State Lett. 14 (5) (2011) A79.
[13] J.S. Chen, T. Zhu, Q.H. Hu, J. Gao, F. Su, S.Z. Qiao, X.W. Lou, ACS Appl. Mater. Interfaces 2 (2010) 3628.
[14] P. Zhang, Z.P. Guo, Y. Huang, D. Jia, H.K. Liu, J. Power Sources 196 (2011) 6987.
[15] Y. Fan, H. Shao, J. Wang, L. Liu, J. Zhang, C. Cao, Chem. Commun. 47 (2011) 3469.
[16] Y. Li, B. Tan, Y. Wu, Nano Lett. 8 (2008) 265.
[17] J. Ryu, S.W. Kim, K. Kang, C.B. Park, ACS Nano 4 (2010) 159.
[18] N. Du, H. Zhang, B. Chen, J. Wu, X. Ma, Z. Liu, Y. Zhang, D. Yang, X. Huang, J. Tu, Adv. Mater. 19 (2007) 4505.
[19] Y. Wang, H. Xia, L. Li, J. Lin, ACS Nano 4 (2010) 1425.
[20] K.M. Shaju, F. Jiao, A. Debart, P.G. Bruce, Phys. Chem. Chem. Phys. 9 (2007) 1837.
[21] Z.W. Zhao, Z.P. Guo, H.K. Liu, J. Power Sources 147 (2005) 264.
[22] F. Li, Q.Q. Zou, Y.Y. Xia, J. Power Sources 177 (2008) 546.
[23] X.W. Lou, D. Deng, J.Y. Lee, J. Feng, L.A. Archer, Adv. Mater. 20 (2008) 258.
[24] X.W. Lou, D. Deng, J.Y. Lee, L.A. Archer, J. Mater. Chem. 18 (2008) 4397.
[25] X.W. Lou, D. Deng, J.Y. Lee, J. Feng, L.A. Archer, Chem. Mater. 20 (2008) 6562.
[26] R. Yang, Z. Wang, J. Ziu, L. Chen, Electrochem. Solid-State Lett. 7 (12) (2004) A496.
[27] W. Yang, N.L. Xu, J. Chen, Adv. Funct. Mater. 15 (2005) 851.
[28] S. Laruelle, S. Grugeon, P. Poizot, M. Dolle, L. Dupont, J.M. Tarascon, J. Electrochem. Soc. 149 (2002) A627.
[29] J. Jamnik, J. Maier, Phys. Chem. Chem. Phys. 5 (2003) 5215.
[30] J. Hu, H. Li, X. Huang, L. Chen, Solid State Ionics 177 (2006) 2791.